NeuroImage: Clinical 34 (2022) 103013

Contents lists available at ScienceDirect

NeuroImage: Clinical

journal homepage: www.elsevier.com/locate/ynicl

Thalamic structural connectivity profiles in blepharospam/ Meige's syndrome

Tobias Mantel [a,1], Angela Jochim [a,1], Tobias Meindl [a], Jonas Deppe [a], Claus Zimmer [b], Yong Li [a], Bernhard Haslinger [a,*]

[a] Department of Neurology, Klinikum rechts der Isar, Technische Universität München, Ismaninger Strasse 22, Munich, Germany
[b] Department of Neuroradiology, Klinikum rechts der Isar, Technische Universität München, Ismaninger Strasse 22, Munich, Germany

ARTICLE INFO

Keywords:
Focal dystonia
Diffusion tractography
Thalamus connectivity mapping
Blepharospasm

ABSTRACT

Background: Blepharospasm is a debilitating focal dystonia characterized by involuntary eyelid spasms that can be accompanied by oromandibular muscle involvement (Meige's syndrome). Frequently observed abnormality in functional neuroimaging hints at an important position of the thalamus, that relays involved cortico-basal ganglia-cortical and cortico-cerebello-cortical circuits, within the abnormal network in blepharospasm.
Objective: To characterize abnormal cortico-thalamic structural/streamline connectivity (SC) patterns in the disease, as well as their potential co-occurrence with abnormal subcortico-thalamo-cortical projections using diffusion tractography.
Methods: Diffusion imaging was obtained in 17 patients with blepharospasm (5 with mild lower facial involvement) and 17 healthy controls. Probabilistic tractography was used for quantification of SC between six cortical regions and thalamus, and voxel-level thalamic SC mapping as well as evaluation of the thalamic SC distributions' topography by center-of-gravity analysis was performed. *Post-hoc*, correlations of SC with clinical parameters were evaluated. Further, white matter integrity was investigated within representative segments of the dentato-thalamo-cortical and pallido-thalamo-cortical tract.
Results: Connectivity mapping showed significant reduction of right (pre)motor- and left occipital-thalamic SC, as well as a topographic shift of the left occipital-thalamic SC distribution in patients. Significant positive correlation of occipital-thalamic SC with disease severity was found. *Post-hoc* analysis revealed significantly reduced mean fractional anisotropy in patients within the dentato-thalamo-cortical trajectory connecting to right (pre) motor and left occipital cortex.
Conclusion: Abnormal occipital/motor SC provides evidence for dysfunction of the thalamus-relayed visual and motor network as a key aspect in the disease. Concurrent impairment of microstructural integrity within the dentato-thalamic trajectories targeting those cortices hints at cerebellar contribution.

1. Introduction

Blepharospasm is a frequent focal dystonia characterized by disabling involuntary blinking and eyelid spasms leading to functional blindness in its most severe form (Valls-Sole and Defazio, 2016). In up to 50% of cases additional involvement of contiguous muscles mainly in the oromandibular region may occur, then labeled Meige's syndrome (Berman et al., 2020; Pandey and Sharma, 2017). First-choice symptomatic treatment is regular local botulinum toxin A (BoNT-A) injection into overactive muscles (Colosimo et al., 2010). While dystonia has traditionally been described as a disorder mainly caused by altered basal ganglia function, the common view of the pathophysiology has shifted in recent years towards the interpretation as a network disease. Beyond the basal ganglia, such network concept includes sensory and motor cortical areas, thalamus, cerebellum and brainstem (Mascia et al., 2020). Clinical dystonia is thought to result from dysfunctional

Abbreviations: BDS, blepharospasm disability scale; BoNT-A, botulinum toxin A; CoG, center of gravity; CON, healthy controls; JRS, Jankovic rating scale; PAT, blepharospasm/Meige's syndrome patients; SC, streamline/structural connectivity; TFCE, threshold-free cluster enhancement.

* Corresponding author at: Klinik und Poliklinik für Neurologie, Klinikum rechts der Isar, Technische Universität München, München, Germany.
E-mail address: bernhard.haslinger@tum.de (B. Haslinger).

[1] These authors contributed equally.

https://doi.org/10.1016/j.nicl.2022.103013
Received 19 December 2021; Received in revised form 18 April 2022; Accepted 19 April 2022
Available online 22 April 2022

interaction of the networks' brain regions, possibly with weighted type-associated involvement (Jinnah et al., 2017). In blepharospasm, retrospective studies/case summaries on its acquired form report lesions with thalamic involvement with considerable frequency, followed by basal ganglia, brainstem, and other lesions within the above network (Khooshnoodi et al., 2013; Mascia et al., 2020). Past functional neuroimaging studies conducted in the idiopathic form frequently and consistently observed abnormal thalamic activation (Baker et al., 2003; Emoto et al., 2010; Murai et al., 2011; Obermann et al., 2008; Suzuki et al., 2019; Suzuki et al., 2007). Accordingly, supported by its role in relaying (among others) the cortico-basal ganglia-cortical and cortico-cerebello-cortical circuits (Conte et al., 2020; Jinnah et al., 2017) that display abnormal functional connectivity (FC) profiles in blepharospasm (Jochim et al., 2018a; Ni et al., 2017), the thalamus has been proposed as a potential key hub in the blepharospasm network (Mascia et al., 2020). Yet, it remains to date ultimately unknown if the projections between thalamus and cortex within such proposed network are abnormal in idiopathic blepharospasm. The present study therefore aimed at elucidating the structural connectivity pattern between thalamus and cortex in the disease. We hypothesized to observe bilateral alterations of thalamic connectivity in projections involved in sensorimotor and/or visuomotor processing (i.e. (pre)motor, somatosensory, posterior parietal, occipital) that are discussed dysfunctional in the disease, without assumptions regarding directionality. We were further interested if potential findings were accompanied by impaired white matter integrity in ascending projections from basal ganglia and cerebellum that are relayed via the thalamus.

2. Materials and methods

2.1. Participants

Seventeen patients (PAT; age 62.2 ± 10.7 years, male/female 10/7) and 17 age- and sex-matched healthy controls (CON; age 62.4 ± 10.2 years, male/female 10/7) were investigated. Twelve patients suffered from isolated blepharospasm. Five had mild additional involvement of the lower face mimic/orbicularis oculi muscles not requiring treatment (i.e. Meige's syndrome). PAT were recruited from the movement disorders outpatient clinic of the Department of Neurology, Klinikum rechts der Isar, Technical University of Munich. Diagnosis had previously been made by a movement disorders expert neurologist. All participants were right-handed (Oldfield, 1971), with no relevant structural abnormalities on MRI by neuroradiologic evaluation (see supplement for further inclusion/exclusion details). All patients received regional periorbital BoNT-A injections in regular intervals (Table 1); MRI measurements were performed prior to the next planned BoNT-A injection after the effect had waned. The study protocol was approved by the local ethics committee (https://www.ek-med-muenchen.de). Written informed consent according to the Declaration of Helsinki was obtained from all participants. Patients were videotaped to assess disease-related impairment using the Jankovic Rating Scale (JRS), an external rating of symptom severity and frequency, calculated as sum score from ratings between "0″ (no symptoms) to "4" (severe or very frequent eyelid spasms) (Jankovic and Orman, 1987). The rater (B.H.) was blinded to neuroimaging analysis results and treatment status. Further, patients' subjective impairment was evaluated using the Blepharospasm Disability Scale (BDS). In this questionnaire, the patient is asked to rate the functional impairment in eight specific situations of daily life, resulting in a sum score of 100% (no impairment) or lower (Lindeboom et al., 1995). Thirteen of the 17 PAT had been previously examined using resting state fMRI reported elsewhere (Jochim et al., 2018a).

Table 1
Demographic and clinical characteristics.

	Dystonia patients (n = 17)	Healthy controls (n = 17)	p-value
Age, years (mean, SD)	62.2, 10.7	62.4, 10.2	0.95[1)]
Sex (male/female)	10/7	10/7	1.0[2)]
TIV, cm^3 (mean, SD)	1421.2, 105.5	1478.9, 110.3	0.13[1)]
Disease duration, years (mean, SD)	9.24, 6.51	–	
Light sensitivity (yes/no)	14/3		
Treatment duration, years (mean, SD)	6.74, 6.72	–	
Interval since last treatment, weeks (mean, SD)	12.4, 1.79	–	
Treatment doses, MU (mean, SD)			
-Onoabotulinumtoxin (Botox®, 7 patients)	43.00, 13.88	–	
-Incoboutlinumtoxin (Xeomin®, 3 patients)	66.5, 9.97		
-Abobotulinumtoxin (Dysport®, 7 patients)	162.86, 31.94		
Blepharospasm Disability Scale (median, IQR / mean, SD)[b]	0.48, 0.24 / 0.51, 0.23	–	
Jankovic Rating Scale (median, IQR / mean, SD)	5, 3 / 4.35, 2.74	–	

Demographic and clinical characteristics of orofacial dystonia patients and healthy controls. Statistical between-group comparisons of demographic characteristics were conducted using [1)]t-tests and [2)]Wilcoxon-Mann-Whitney tests. SD = standard deviation; IQR = interquartile range; MU, mouse units; y = years; h = hours; TIV = total intracranial volume; m = male; f = female.

2.2. MRI data acquisition and preparation

Acquisition. Data were acquired on a 3 T Achieva MRI scanner (Philips, the Netherlands) with an 8-channel head coil. Software for data analysis is detailed in supplemental table s-1. 64-gradient direction diffusion tensor MR images were acquired using a cardiac-gated single-shot spin-echo echo-planar imaging sequence (echo time = 92 ms, (heart rate-dependent) repetition time = 11–22 bpm, b-value = 1400 s/mm^2, α = 90°; field-of-view = 232 × 232 mm; voxel size = 1.81 × 1.81 × 2 mm^3; 66 axial slices without gap, 2 b0 total, (heart rate-dependent) overall scan time 30–36 min). Participants' heads were fixed with foam pads to minimize risk of motion artefacts. To further reduce motion risk in view of relatively long scan durations owed to cardiac gating, image acquisition was divided into two separate runs of 32 diffusion-weighted images each. Additionally, a high-resolution 3D gradient-echo T1 for anatomical reference, and a 2D FLAIR (for neuroradiological evaluation) were acquired.

Preparation. Diffusion MRI data from both sessions were concatenated, corrected for motion/eddy current-induced geometrical distortions, and for susceptibility-induced distortion aided by information from the aligned anatomical scan with upsampling to a voxel size of 1 mm isotropic (Irfanoglu et al., 2012; Leemans and Jones, 2009). Proper alignment of diffusion and anatomical scan was visually checked independently by two experienced neuroscientists (A.J./T.M.). Data quality control included visual checks of structural data integrity and of fitting residuals, evaluation of motion, and of voxel outliers of the diffusion tensor fit (table s-2). For probabilistic tractography preparation, FSL's *bedpostx* was applied to model two crossing fibers/voxel after automatic voxel-wise determination of the number of crossing fibers (Behrens et al., 2007; Jbabdi et al., 2012; Jenkinson et al., 2012). T1 scans were tissue-segmented using CAT12 for use in tractography and morphometric control analyses (see supplement for details) (Gaser and Dahnke, 2016).

2.3. Seed-based probabilistic tractography mapping of thalamic connectivity profiles

Probabilistic tractography (henceforth 'tractography') was performed as implemented in the FSL probabilistic fiber tracking tool (*probtrackx2*) to reconstruct the probable diffusion trajectories between the prefrontal, motor/premotor, (somato)sensory, posterior-parietal, occipital, temporal cortices and the thalamus separately for each

hemisphere in the native space of each participant (Behrens et al., 2007; Behrens et al., 2003a; Behrens et al., 2003b). All regions of interest (ROIs, figure s-1) were derived from the Brainnetome atlas parcellation (Fan et al., 2016), that provides detailed structural/streamline (SC)-based brain segmentation making it suitable for this purpose. Cortical ROIs were defined in accordance with previous similarly conceived studies in line with known connectional anatomy (Jones, 2007; Nair et al., 2013; Zhang et al., 2010). Some of those studies had investigated connectivity profiles of the posterior-parietal and occipital lobe either separately (Behrens et al., 2003a; Giraldo-Chica et al., 2018) or in combination (Nair et al., 2013; Zhang et al., 2010). We opted for the separate approach to discriminate potential parietal and occipital findings in light of previous functional neuroimaging observations of both abnormal connectivity profiles of occipital cortices at rest (Jochim et al., 2018a), and abnormal occipital activity in task activation studies related to blinking (Baker et al., 2003; Nguyen et al., 2020) or visual processing (Suzuki et al., 2019). The thalamic target ROI comprised the entire thalamus including the corpus geniculatum mediale et laterale. Tractography was performed in the respective participant's native space and all required ROIs/masks registered accordingly applying the inverse transformation parameters derived from (linear and nonlinear) registration of the anatomical scan to Montreal Neurologic Institute (MNI) standard space (Behrens et al., 2003b). Trajectories were seeded from the grey-matter-white-matter interface (5,000 streamlines/voxel) of each cortical seed ROI and separately for each hemisphere as done in other work (Nair et al., 2013), anatomically-constrained to the ipsihemispheric white matter. Exclusion masks were set to eliminate potential fiber propagation through brainstem/cerebellum/basal ganglia. Tractography was performed using standard parameters and loopcheck (curvature threshold 0.2, maximum number of steps 2000, step length 0.5 mm, subsidiary fiber volume threshold 0.01). Distance correction was applied to account for the fact that connectivity distribution drops with distance from the seed mask.

The above tractography procedure generates voxel-wise probabilities of an existing path between the cortical seed ROIs and the thalamus (used as waypoint target ROI) in each hemisphere in each subject as a surrogate measure of white matter connectivity (Behrens et al., 2007; Jbabdi and Johansen-Berg, 2011; Zhang et al., 2010). To enable inter-subject comparability, those voxel-wise connection probabilities in the individual streamline density maps were normalized by the total number of valid streamlines in each individual tractography ("*waytotal*"), taking into account inter-subject variabilities including differing ROI-sizes and the use of exclusion masks (Zhang et al., 2010). Then, these voxel maps containing the information about the normalized connection probability (structural/streamline connectivity) for each cortical seed ROI were registered to standard space for identification of thalamic areas exhibiting group differences, and for correlation analyses.

2.4. Topographic evaluation of thalamic connectivity profiles

To additionally evaluate for potential topographic differences in thalamic SC distribution patterns, we extracted the distribution's center of gravity (CoG) as a surrogate marker for each cortical thalamic SC profile (prefrontal, motor/premotor, (somato)sensory, posterior-parietal, occipital, temporal) in each subject. The CoG (with SC values substituted for mass in this situation) for a given thalamic SC distribution is a 3D space coordinate that is calculated as the weighted average of the coordinates of all voxels in that thalamic SC distribution (Behrens et al., 2003a). The CoG therefore is (by contrast to the maximum coordinate) representative of the overall intra-thalamic spatial connection pattern with the underlying cytoarchitecture. The measure has been demonstrated to relate both to underlying histology and to function in SC-based analyses, and has been applied as in previous tractography-based analyses of subcortical/cortical SC patterns (Anwander et al., 2007; Bertino et al., 2020; Devlin et al., 2006; Johansen-Berg et al., 2004).

2.5. Post-hoc evaluation of cerebello- and pallido-thalamic fiber integrity

For cortices with abnormal group thalamic SC profiles, we evaluated the microstructural integrity within the efferent sections of cortico-basal ganglia-cortical and cortico-cerebellar circuits that are relayed via the thalamus. Details are outlined in the supplementary methods. In brief, we applied a previously employed anatomically-constrained tractography approach to reconstruct the dentato-thalamo-cortical tract (DTCT) and the pallido-thalamo-cortical tract (PTCT) in each participant, respectively seeding from either the contralateral dentate area in the cerebellum or the ipsilateral pallidum to the grey matter-white matter interface of the respective cortex of interest. Resulting projections were thresholded across a number of commonly used connection probability thresholds. Tracking through bottleneck sections and/or fibre crossings along the tracts' courses in the narrow brainstem may technically bias SC values and affect spatial accuracy of subsequent tract reconstruction (Jones, 2010; Mangin et al., 1996). We therefore focused on the analysis of FA as reliable measure of white matter integrity as sensitive and (especially in the subcortical domain (Luque Laguna et al., 2020)) reliable measure of fiber integrity in a representative tract segment. Accordingly, mean FA was extracted in the native space from the tract segments across thresholds (see figure s-3), averaged, and screened for potential group differences.

2.6. Statistical design and control analyses

The primary statistical analysis focused on the detection of local (i.e. voxel-level) between-group differences in thalamic SC. Statistical analysis was performed applying nonparametric permutation testing according to the Freedman-Lane approach (5,000 permutations) with threshold-free cluster enhancement (TFCE) (Salimi-Khorshidi et al., 2011; Smith and Nichols, 2009), family-wise error (FWE) corrected for multiple comparisons at the voxel level (Holmes et al., 1996; Winkler et al., 2016; Winkler et al., 2014). Beyond avoiding assumptions on data distribution, TFCE is robust to non-stationarity requiring only minimal pre-smoothing, and avoids arbitrary cluster-forming thresholds (Eklund et al., 2016). To maximize statistical power, the corresponding left and right-hemispheric normalized connectivity maps for a given cortical ROI were analyzed in combination. Analyses were masked to include only voxels with an average relative connection probability greater than 10% for a given projection (Giraldo-Chica et al., 2018). Probability maps were slightly pre-smoothed (4 mm Gaussian kernel) to minimize noise. Results were deemed significant surviving Bonferroni-adjustment for the total number of analyses performed ($p_{FWE(TFCE)} < 0.05/6$). To aid interpretation of results from a descriptive standpoint, we additionally characterized the ipsihemispheric cortical SC profile of those thalamic voxels showing significant between-group difference across all study participants (see supplement/figure s-2 for details). Further, abnormalities in topography mirrored by differences in the centers of gravity of the thalamic connectivity distributions as surrogate marker were tested for significant GROUP × COORDINATE interaction effects using multivariate ANOVAs (factors: GROUP, COORDINATE; variates: CoG coordinates for a given cortical ROI in each hemisphere) at a corresponding Bonferroni-corrected significance-level of $p < 0.05/6$. Significant results were followed by separate two-way ANOVAs for each hemisphere ($p < 0.05/2$) with planned simple effects analyses to look into differences at the coordinate level, adjusted for the 3D space ($p < 0.05/3$) (Fisher, 1992). Co-occurrence of significant topographic shifts with local SC abnormalities in the primary analysis were followed up with a between-group comparisons of the average SC within the thalamic ROI for further characterization (Wilcoxon-Mann-Whitney test, $p < 0.05$) (Mann and Whitney, 1947).

Second, *post-hoc* secondary exploratory analyses were conducted for further characterization of significant results in the primary analysis. (i) Potential group differences in microstructural integrity by FA within representative segments of the probable trajectories of the DTCT and

PTCT were investigated (Wilcoxon-Mann-Whitney test, $p < 0.05$). (ii) Correlations with three clinical parameters (disease severity by JRS and BDS, age at onset) were calculated (Spearman's ρ, $p < 0.05/3$) (Spearman, 1904).

3. Results

3.1. Thalamic structural connectivity mapping

SC mapping (Fig. 1) revealed a significantly reduced left occipital-thalamic SC in PAT (x|y|z = -16|-30|8, $t_{TFCE} = 102.04$, $p_{FWE(TFCE)} = 0.001$, cluster size = 192 mm^3). Further, right motor/premotor-thalamic SC was reduced (x|y|z = 14|-12|8, $t_{TFCE} = 88.79$, $p_{FWE(TFCE)} = 0.007$, cluster size = 8 mm^3). The descriptive reverse tracking control analysis

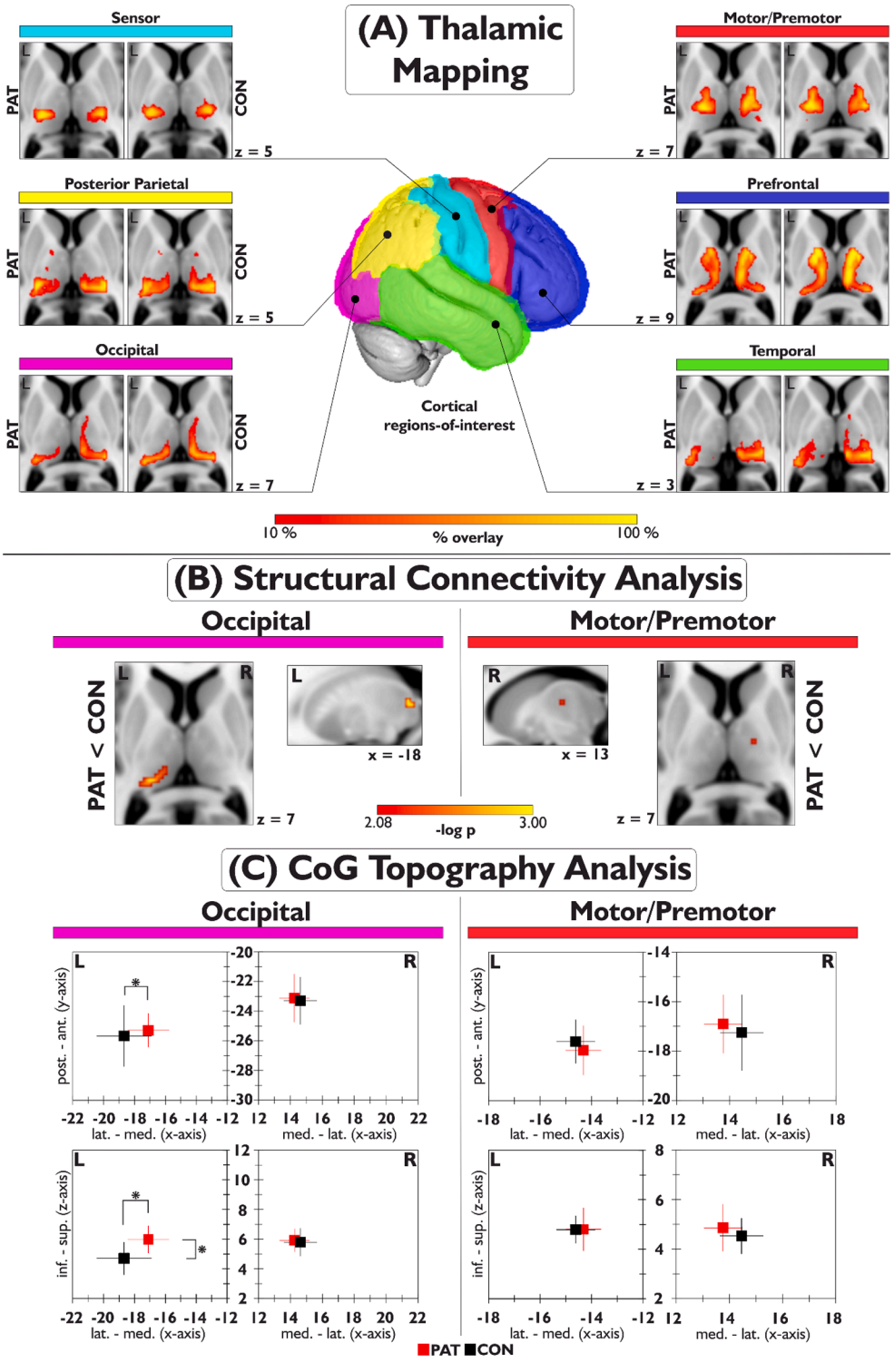

Fig. 1. Results of the thalamic SC mapping analysis in blepharospasm/Meige's syndrome patients and healthy controls, displayed in neurological convention in standard (MNI) space. *Section A:* Individual group results of the thalamic connectivity mapping for each of the six investigated cortical regions of interest in each hemisphere. Colorbar indicates percent overlay of trajectories across participants in each group at an average connection probability threshold of 10%. *Section B:* Significant local SC group differences found for the motor/premotor and occipital SC distributions ($p_{FWE(TFCE)} < 0.0083$ (0.05/6). *Section C*: the corresponding results of the topographic analysis calculated from the unthresholded thalamic SC distribution's centers of gravity (CoGs) as surrogate marker. Asterisks highlight significant differences. PAT, dystonia patients; CON, healthy controls; L, left hemisphere, R, right hemisphere.

from these significant voxels indicated that the (pre)motor thalamic cluster was mainly connected to the supplementary motor, dorsal premotor area and motor cingulum. The occipital thalamic cluster had rather distributed occipital connectivity profile with emphasis on cuneus, lateral/superior occipital cortex and the parieto-occipital sulcus area (fig. s-2). The amount of grey and white matter within the thalamic ROIs did not differ between groups (Wilcoxon-Mann-Whitney test, total intracranial volume (TIV)-normalized volumes; all $z<|0.98|$, all $p > 0.34$). Average thalamic SC values were not associated with the amount of thalamic grey and white matter (all $\rho<|0.12|$, all $p > 0.51$).

3.2. Topographic evaluation of thalamic SC profiles

Group comparison of CoGs revealed a significant GROUP × COORDINATE interaction effect for the occipital thalamic SC distribution ($F_{4,192} = 3.81$, $p = 0.005$) attributable to the left hemisphere ($F_{2,96} = 8.29$, $p < 0.001$, partial $\eta^2 = 0.15$), indicating a group topographic difference in the left occipital SC distribution (Fig. 1/table s-2). Simple effects analysis suggested this was owed to a medio-superior CoG shift in PAT (x/y/z-axis $p = 0.0021/0.43/0.012$; Fig. 1). Adjunct between-group analysis of mean left thalamic occipital lobe SC within the thalamic ROI - conducted in light of the co-occurrence of local SC and CoG abnormality - showed a significant mean SC reduction in PAT consistent with the voxel-wise main analysis ($z = -2.78$, $p = 0.0047$). This indicated that the local difference observed in the main analysis was not explained by the shift in CoGs. Otherwise, no significant differences were found.

3.3. Post-hoc exploratory evaluation of occipital/motor cerebello- and pallido-thalamic fiber integrity

Post-hoc evaluation of structural integrity in representative segments of the DTCT and PTCT revealed significantly reduced mean FA in PAT within the probable DTCT trajectories connecting to the right motor/premotor ($z = -2.29$, $p = 0.022$, effect size $r = 0.39$) and left occipital cortex ($z = -2.13$, $p = 0.033$; $r = 0.37$; Fig. 2), and no significant group differences for the PTCT (all $p > 0.16$, all $z<|1.43|$).

3.4. Post-hoc correlation of abnormal occipital/motor thalamic SC with clinical parameters

Average SC of voxels within the occipital thalamic SC cluster showed a significant moderate positive correlation with the JRS-based grading of disease severity by blinking frequency and spasm severity ($\rho = 0.58$; $p = 0.014$), but not with BDS-defined disease-related impairment ($\rho = -0.34$, $p = 0.18$). No significant correlation with age of disease onset, and no significant correlations for the motor/premotor thalamic SC cluster were observed (all $\rho<|0.33|$, all $p > 0.20$).

4. Discussion

The present study showed reductions of left occipital and right motor/premotor thalamic SC in patients with blepharospasm. Mapping of the thalamus according to its probable white matter connections has previously been applied in several neurologic/neuropsychiatric diseases with suspected thalamic involvement (Giraldo-Chica et al., 2018; Nair et al., 2013). Work in the healthy suggests that such diffusion imaging-based mappings of grey matter structures show spatial similarity to underlying histology (i.e. accordingly connected areas) (Jbabdi and Johansen-Berg, 2011), yet we emphasize thalamic mappings as performed here do not generate individual hard anatomical segmentations/labels of the single thalamic subnuclei (Clayden et al., 2019). The thalamic (pre)motor SC distribution in the present study was centered in the ventral (anterolateral) thalamus while the one generated from occipital projections was centered in the posterior thalamus. This is consistent both with previous studies (Behrens et al., 2003a; Giraldo-Chica et al., 2018; Nair et al., 2013; Zhang et al., 2010), and with the broader spatial distribution of thalamic nuclear areas accordingly involved in the processing of these modalities. Further, an additional reverse-tracking control analysis across participants confirmed a predominant link of significantly abnormal thalamic (pre)motor and

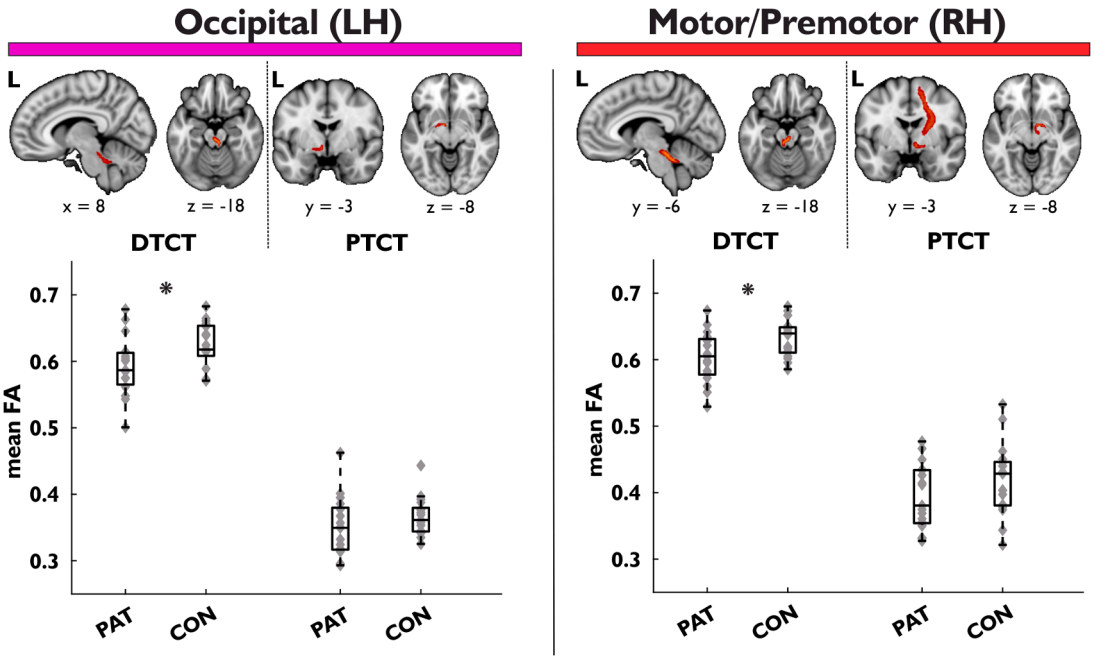

Fig. 2. Results of *post-hoc* reconstruction and group comparison of the probable trajectories of the dentato-thalamo-cortical tract (DTCT) and the pallido-thalamo-cortical tract (PTCT) targeting the left occipital and the right motor/premotor cortex respectively. *Upper panel:* Overview over subcortical sections of reconstructed projections (for more extensive depiction, see supplemental figure s-3). For visualization purpose, images were thresholded to show voxels shared among at least 4/34 participants at a connection probability threshold of 5%. *Lower panel*: Results of the group comparison of average FA in representative tract segments, visualized as box plots (maximum whisker length = 1.5*IQR), with grey diamonds indicating single values. Asterisks marks significant ($p < 0.05$) group differences in the nonparametric statistical analysis. PAT, dystonia patients; CON, healthy controls; FA, fractional anisotropy; L(H), left hemisphere; R(H), right hemisphere.

occipital voxels with the (pre)motor cortices (especially right supplementary motor, dorsal premotor area and motor cingulum), and occipital cortices respectively (with some emphasis on cuneus, lateral/superior occipital cortex and the area around the parieto-occipital sulcus).

Based on our information, a specific analysis of thalamic SC profiles using connectivity mapping has not been undertaken before in dystonia. In the healthy, the thalamus is a key integrative hub, gating both ascending pathways (from periphery, brainstem nuclei, basal ganglia, cerebellum) as well as distinct cortico-cortical projections (Guillery and Sherman, 2002; Hintzen et al., 2018; Hwang et al., 2017). In our work, (pre)motor SC was found reduced in the right thalamus. (Pre)motor thalamic projections mediate cerebellar and basal ganglia control of cortical excitability/surround inhibition and cortical plasticity that are considered defective in dystonia, ultimately leading to motor overflow (Quartarone and Hallett, 2013). Previous resting-state fMRI in a subset of participants of the present work hinted at potential modulation of FC between ipsilateral cingulate/supplemental motor area and right thalamus by BoNT-A, though directionality remains unclear (Jochim et al., 2018a). We further observed reduced left occipital thalamic SC. Regarding functional abnormality in occipital cortices, early event-related functional MRI studies hinted at abnormal involvement in primary/and or associative visual cortices within an abnormally activated visuomotor network related to simple blinking tasks (further including anterior cingulum, primary motor cortex, basal ganglia, and superior cerebellum) (Baker et al., 2003). Recently, increased activity in the occipital associative cortex (in addition to increased primary somatosensory, motor cortical and cerebellar activity) has additionally been demonstrated during reflexive blinking (Nguyen et al., 2020). While increases in visual input interruption in blepharospasm (mirrored by disease severity) and the resulting reduction in quantitative visual input are assumed to lead to reduced relative visual cortex glucose metabolism over time as secondary phenomenon (Suzuki et al., 2019), it remains to date unclear if quantitively comparable visual input is processed differently in the disease. The observation of anticorrelation of increased occipital cortex activity during reflexive blinking with disease severity may hint at a context-related dimension of functional abnormality in the occipital cortices. Further, seed-based FC in the eyes-closed resting state indicated decreased cerebellar and basal ganglia FC to the occipital association cortices that were equally not explained by disease-related impairment (Jochim et al., 2018a). Our observation of occipital-thalamic SC supports a role of thalamus-relayed projections with regard to these described functional occipital abnormalities seen in the disease.

Interestingly, occipital thalamic SC reduction in our study was relatively less pronounced in more severely affected patients. Previous functional neuroimaging studies indicated that thalamic activity increases with disease severity during various tasks (Murai et al., 2011; Suzuki et al., 2019). Yet, the multimodality (motor, multi-sensory) of processed information in these paradigms together with the fMRI techniques' limitation to identify the underlying process makes direct deductions regarding our present finding difficult. Information relayed via the thalamus to the occipital (or other) cortex undergoes modulatory influence from the cortex it is projected to, as well as from other higher-order brain areas and/or from thalamic nuclei/interneurons (Guillery and Sherman, 2002). This may indicate that our observation could reflect the presence of either a maladaptive, or a broken-down compensatory process. As diffusion imaging cannot discern functionally distinct fiber subpopulations within the occipital radiation, this warrants further research on thalamus-related network dynamics in the disease.

Altogether, the observation of structural occipital and motor cortical thalamic dysconnectivity supports a role also of the thalamocortical segment within the dystonia network. Such notion would fit well with observations in limb dystonia suggesting that abnormal microstructure within motor thalamocortical (and not corticostriatal) pathways may determine the limb phenotype (Vo et al., 2015). Given the limitations inherent to neuroimaging, we cannot discern if the observed thalamic abnormality is of causative or compensatory/adaptive nature. The thalamus functions as a hub that relays and converges, but is also modulated by its afferences (Aumann, 2002; Hintzen et al., 2018; Kaas, 1999; Silkis, 2001) making it subject to complex influences, and tractography cannot provide information on fiber directionality (Behrens et al., 2003a). Further, it remains to date unclear if altered connectivity as observed here is determined by a differing number of axons, affection of myelinization, axon spreading or other reasons.

An intriguing new observation was an additional topographic shift of the left occipital thalamic SC distribution in patients. While topographic shifts of functional body-part representations within somatosensory cortices have consistently been demonstrated across other forms of focal dystonia and discussed as an indirect correlate of maladaptive plasticity demonstrated in electrophysiological studies in focal dystonia (Neychev et al., 2011), this has to our knowledge to date not been the case for blepharospasm, the thalamus or the visual sensory modality using neuroimaging. The observation of abnormality in the visual sensory modality is conceptually congruent with early observations during thalamic micro-stimulation indicating reorganization of sensory thalamic maps in upper-limb dystonia as a potential contributor to overflow of muscle activation (Lenz et al., 1999); yet, the question may arise why thalamic SC abnormalities were not identified for somatosensory cortex connections in the present study. In light of a less prominent clinical involvement compared to the visual system in blepharospasm, a reduced sensitivity of our approach in detecting those changes compared to visual sensory abnormalities (e.g. possibly owed to a less pronounced structural aspect of thalamic reorganisation in the somatosensory domain) may be conceivable.

To explore the potential co-occurrence of our occipital/ (pre)motor thalamic findings with microstructural abnormality of major thalamic afferences originating from cerebellum and basal ganglia - both assumed to play a key role within the dystonia network concept (Jinnah et al., 2017) - we conducted a planned secondary analysis investigating the microstructural integrity of the thalamus-relayed dentato- (rubro)-thalamo-cortical and pallido-thalamo-cortical trajectories (Aumann, 2002; Hintzen et al., 2018; Kaas, 1999; Silkis, 2001). This secondary analysis indicated abnormal microstructural integrity mirrored by FA reduction within the DTCT connecting the dentate (via the thalamus) to the right (pre)motor and left occipital cortex, that had both displayed thalamic SC abnormalities in the primary analysis. Given the inherent limitations of neuroimaging, further experimental studies may be needed to clarify if such coherence indeed translates into interactions at the histological level. While work in hereditary dystonia with cranial involvement reported cerebello-thalamic tract abnormalities (Argyelan et al., 2009; Jochim et al., 2018b), tractography studies are to date sparse in idiopathic blepharospasm. One ROI-based diffusion study in blepharospasm found abnormal cerebellar FA but did not perform tractography (Yang et al., 2014). Though our observation is intriguing, confirmation in follow-up studies is warranted given this evaluation of DTCT and PTCT constituted a secondary analysis.

In our study, we did not observe bilateral abnormality of occipital and motor projections. The descriptive nature of neuroimaging studies limits direct inferences regarding the underlying causes of such lateralization, that are frequently observed also in clinically bilateral forms of dystonia including blepharospasm. We emphasize that our observations naturally do not preclude bilateral abnormality, as sensitivity for any neuroimaging finding may be influenced by factors on such as methodological aspects, varying magnitude of the underlying effect (also as consequence physiological or disease-related asymmetries), or other. From a methodological point of view, a comparatively small number of the subjects examined may have led to limited sensitivity and was owed to the fact that in addition to focal dystonia being a rare disease, the MRI study eligibility is even more narrowed down due to the increased age of onset in this form of dystonia compared to other types (accompanied by

an increased prevalence of relevant cerebral lesions and concomitant diseases). With regard to a potential relationship of structural lateralization with anomalies in lateralized functional networks, the inferences from structural imaging on their specific embedding in such functional networks are inherently limited. To provide some perspective regarding reported hemispheric lateralization in function networks of potential relevance in the disease, right motor lateralization has been observed in studies on cerebral lesions impairing eyelid function and neuroimaging studies in volitional and spontaneous blinking (Hanakawa et al., 2008; van Eimeren et al., 2001; Yoon et al., 2005). Left occipital lateralization is seen during left-lateralized complex task- and attention-dependent visual processing, and left lateralized functional occipital abnormality has been reported across previous fMRI studies in blepharospasm (Jiang et al., 2019; Kerrison et al., 2003; Nguyen et al., 2020).

5. Conclusion

Altogether, thalamic occipital and (pre)motor structural dysconnectivity with the cortex support the concept of abnormal sensory (visual) processing and dysfunctional ascending motor control via the thalamus within the pathologic network in blepharospasm. Secondary findings suggest concurrent microstructural abnormalities of the respective cerebellar afferent projections routed through the thalamic network node.

Funding

This study was supported by the Deutsche Forschungsgemeinschaft (DFG HA3370/5-1) Bonn, Germany.

CRediT authorship contribution statement

Tobias Mantel: Conceptualization, Methodology, Formal analysis, Visualization, Writing – original draft, Writing – review & editing. **Angela Jochim:** Conceptualization, Investigation, Formal analysis, Writing – original draft, Writing – review & editing. **Tobias Meindl:** Writing – review & editing. **Jonas Deppe:** Writing – review & editing. **Claus Zimmer:** Resources, Writing – review & editing. **Yong Li:** Investigation, Data curation, Writing – review & editing. **Bernhard Haslinger:** Conceptualization, Funding acquisition, Resources, Project administration, Supervision, Writing – review & editing.

Declaration of Competing Interest

The authors declare that they have no known competing financial interests or personal relationships that could have appeared to influence the work reported in this paper.

Acknowledgments

We thank with the German Dystonia Society for their support in patient and recruitment and all subjects for their participation and the study.

Appendix A. Supplementary data

Supplementary data to this article can be found online at https://doi.org/10.1016/j.nicl.2022.103013.

References

Anwander, A., Tittgemeyer, M., von Cramon, D.Y., Friederici, A.D., Knosche, T.R., 2007. Connectivity-based parcellation of Broca's area. Cereb. Cortex 17, 816–825.
Argyelan, M., Carbon, M., Niethammer, M., Ulug, A.M., Voss, H.U., Bressman, S.B., Dhawan, V., Eidelberg, D., 2009. Cerebellothalamocortical connectivity regulates penetrance in dystonia. J. Neurosci. 29 (31), 9740–9747.
Aumann, T.D., 2002. Cerebello-thalamic synapses and motor adaptation. Cerebellum 1 (1), 69–77.
Baker, R.S., Andersen, A.H., Morecraft, R.J., Smith, C.D., 2003. A functional magnetic resonance imaging study in patients with benign essential blepharospasm. J. Neuroophthalmol. 23 (1), 11–15.
Behrens, T.E.J., Berg, H.J., Jbabdi, S., Rushworth, M.F.S., Woolrich, M.W., 2007. Probabilistic diffusion tractography with multiple fibre orientations: What can we gain? Neuroimage 34 (1), 144–155.
Behrens, T.E.J., Johansen-Berg, H., Woolrich, M.W., Smith, S.M., Wheeler-Kingshott, C. A.M., Boulby, P.A., Barker, G.J., Sillery, E.L., Sheehan, K., Ciccarelli, O., Thompson, A.J., Brady, J.M., Matthews, P.M., 2003a. Non-invasive mapping of connections between human thalamus and cortex using diffusion imaging. Nat. Neurosci. 6 (7), 750–757.
Behrens, T.E.J., Woolrich, M.W., Jenkinson, M., Johansen-Berg, H., Nunes, R.G., Clare, S., Matthews, P.M., Brady, J.M., Smith, S.M., 2003b. Characterization and propagation of uncertainty in diffusion-weighted MR imaging. Magn. Reson. Med. 50 (5), 1077–1088.
Berman, B.D., Groth, C.L., Sillau, S.H., Pirio Richardson, S., Norris, S.A., Junker, J., Brüggemann, N., Agarwal, P., Barbano, R.L., Espay, A.J., Vizcarra, J.A., Klein, C., Bäumer, T., Loens, S., Reich, S.G., Vidailhet, M., Bonnet, C., Roze, E., Jinnah, H.A., Perlmutter, J.S., 2020. Risk of spread in adult-onset isolated focal dystonia: a prospective international cohort study. J. Neurol. Neurosurg. Psychiatry 91 (3), 314–320.
Bertino, S., Basile, G.A., Bramanti, A., Anastasi, G.P., Quartarone, A., Milardi, D., Cacciola, A., 2020. Spatially coherent and topographically organized pathways of the human globus pallidus. Hum. Brain Mapp. 41 (16), 4641–4661.
Clayden, J.D., Thomas, D.L., Kraskov, A., 2019. Tractography-based parcellation does not provide strong evidence of anatomical organisation within the thalamus. Neuroimage 199, 418–426.
Colosimo, C., Suppa, A., Fabbrini, G., Bologna, M., Berardelli, A., 2010. Craniocervical dystonia: clinical and pathophysiological features. Eur. J. Neurol. 17 (Suppl 1), 15–21.
Conte, A., Defazio, G., Mascia, M., Belvisi, D., Pantano, P., Berardelli, A., 2020. Advances in the pathophysiology of adult-onset focal dystonias: recent neurophysiological and neuroimaging evidence. F1000Res 9, 67.
Devlin, J.T., Sillery, E.L., Hall, D.A., Hobden, P., Behrens, T.E.J., Nunes, R.G., Clare, S., Matthews, P.M., Moore, D.R., Johansen-Berg, H., 2006. Reliable identification of the auditory thalamus using multi-modal structural analyses. Neuroimage 30 (4), 1112–1120.
Eklund, A., Nichols, T.E., Knutsson, H., 2016. Cluster failure: Why fMRI inferences for spatial extent have inflated false-positive rates. Proc. Natl. Acad. Sci. USA 113 (28), 7900–7905.
Emoto, H., Suzuki, Y., Wakakura, M., Horie, C., Kiyosawa, M., Mochizuki, M., Kawasaki, K., Oda, K., Ishiwata, K., Ishii, K., 2010. Photophobia in essential blepharospasm–a positron emission tomographic study. Mov. Disord. 25 (4), 433–439.
Fan, L., Li, H., Zhuo, J., Zhang, Y.u., Wang, J., Chen, L., Yang, Z., Chu, C., Xie, S., Laird, A.R., Fox, P.T., Eickhoff, S.B., Yu, C., Jiang, T., 2016. The Human Brainnetome Atlas: A New Brain Atlas Based on Connectional Architecture. Cereb. Cortex 26 (8), 3508–3526.
Fisher, R.A., 1992. Statistical methods for research workers. In: Kotz, S., Johnson, N.L. (Eds.), Breakthroughs in Statistics: Methodology and Distribution. Springer New York, New York, NY, pp. 66–70.
Gaser, C., Dahnke, R., 2016. CAT-a computational anatomy toolbox for the analysis of structural MRI data. Hbm 2016, 336–348.
Giraldo-Chica, M., Rogers, B.P., Damon, S.M., Landman, B.A., Woodward, N.D., 2018. Prefrontal-thalamic anatomical connectivity and executive cognitive function in schizophrenia. Biol. Psychiatry 83 (6), 509–517.
Guillery, R.W., Sherman, S.M., 2002. Thalamic relay functions and their role in corticocortical communication: generalizations from the visual system. Neuron 33 (2), 163–175.
Hanakawa, T., Dimyan, M.A., Hallett, M., 2008. The representation of blinking movement in cingulate motor areas: a functional magnetic resonance imaging study. Cereb. Cortex 18 (4), 930–937.
Hintzen, A., Pelzer, E.A., Tittgemeyer, M., 2018. Thalamic interactions of cerebellum and basal ganglia. Brain Struct. Funct. 223 (2), 569–587.
Holmes, A.P., Blair, R.C., Watson, J.D.G., Ford, I., 1996. Nonparametric analysis of statistic images from functional mapping experiments. J. Cereb. Blood Flow Metab. 16 (1), 7–22.
Hwang, K., Bertolero, M.A., Liu, W.B., D'Esposito, M., 2017. The Human Thalamus Is an Integrative Hub for Functional Brain Networks. J. Neurosci. 37 (23), 5594–5607.
Irfanoglu, M.O., Walker, L., Sarlls, J., Marenco, S., Pierpaoli, C., 2012. Effects of image distortions originating from susceptibility variations and concomitant fields on diffusion MRI tractography results. Neuroimage 61 (1), 275–288.
Jankovic, J., Orman, J., 1987. Botulinum A toxin for cranial-cervical dystonia: a double-blind, placebo-controlled study. Neurology 37, 616-623.
Jbabdi, S., Johansen-Berg, H., 2011. Tractography: where do we go from here? Brain Connect. 1 (3), 169–183.
Jbabdi, S., Sotiropoulos, S.N., Savio, A.M., Graña, M., Behrens, T.E.J., 2012. Model-based analysis of multishell diffusion MR data for tractography: how to get over fitting problems. Magn. Reson. Med. 68 (6), 1846–1855.
Jenkinson, M., Beckmann, C.F., Behrens, T.E.J., Woolrich, M.W., Smith, S.M., 2012. FSL. Fsl. Neuroimage 62 (2), 782–790.
Jiang, W., Lan, Y., Cen, C., Liu, Y., Feng, C., Lei, Y., Guo, W., Luo, S., 2019. Abnormal spontaneous neural activity of brain regions in patients with primary blepharospasm at rest. J. Neurol. Sci. 403, 44–49.

Jinnah, H.A., Neychev, V., Hess, E.J., 2017. The anatomical basis for dystonia: the motor network model. Tremor Other Hyperkinet. Mov. (N Y) 7, 506.
Jochim, A., Li, Y., Gora-Stahlberg, G., Mantel, T., Berndt, M., Castrop, F., Dresel, C., Haslinger, B., 2018a. Altered functional connectivity in blepharospasm/orofacial dystonia. Brain Behav. 8, e00894.
Jochim, A., Li, Y., Zech, M., Lam, D., Gross, N., Koch, K., Zimmer, C., Winkelmann, J., Haslinger, B., 2018b. Microstructural white matter abnormalities in patients with COL6A3 mutations (DYT27 dystonia). Parkinsonism Relat. Disord. 46, 74–78.
Johansen-Berg, H., Behrens, T.E.J., Robson, M.D., Drobnjak, I., Rushworth, M.F.S., Brady, J.M., Smith, S.M., Higham, D.J., Matthews, P.M., 2004. Changes in connectivity profiles define functionally distinct regions in human medial frontal cortex. Proc. Natl. Acad. Sci. USA 101 (36), 13335–13340.
Jones, D.K., 2010. Challenges and limitations of quantifying brain connectivity in vivo with diffusion MRI. Imaging Med. 2 (3), 341–355.
Jones, E.G., 2007. The Thalamus. University Press, Cambridge, UK.
Kaas, J.H., 1999. Is most of neural plasticity in the thalamus cortical? Proc. Natl. Acad. Sci. USA 96 (14), 7622–7623.
Kerrison, J.B., Lancaster, J.L., Zamarripa, F.E., Richardson, L.A., Morrison, J.C., Holck, D. E.E., Andreason, K.W., Blaydon, S.M., Fox, P.T., 2003. Positron emission tomography scanning in essential blepharospasm. Am. J. Ophthalmol. 136 (5), 846–852.
Khooshnoodi, M.A., Factor, S.A., Jinnah, H.A., 2013. Secondary blepharospasm associated with structural lesions of the brain. J. Neurol. Sci. 331 (1-2), 98–101.
Leemans, A., Jones, D.K., 2009. The B-matrix must be rotated when correcting for subject motion in DTI data. Magn. Reson. Med. 61 (6), 1336–1349.
Lenz, F.A., Jaeger, C.J., Seike, M.S., Lin, Y.C., Reich, S.G., DeLong, M.R., Vitek, J.L., 1999. Thalamic single neuron activity in patients with dystonia: dystonia-related activity and somatic sensory reorganization. J. Neurophysiol. 82 (5), 2372–2392.
Lindeboom, R., De Haan, R., Aramideh, M., Speelman, J.D., 1995. The blepharospasm disability scale: an instrument for the assessment of functional health in blepharospasm. Mov. Disord. 10 (4), 444–449.
Luque Laguna, P.A., Combes, A.J.E., Streffer, J., Einstein, S., Timmers, M., Williams, S.C. R., Dell'Acqua, F., 2020. Reproducibility, reliability and variability of FA and MD in the older healthy population: A test-retest multiparametric analysis. Neuroimage Clin. 26, 102168.
Mangin, J., Regis, J., Frouin, V., 1996. Shape Bottlenecks and Conservative Flow Systems. IEEE Workshop on Mathematical Methods in Biomedical Image Analysis. IEEE Computer Society, 1996, San Francisco, pp. 131-138.
Mann, H.B., Whitney, D.R., 1947. On a Test of Whether one of Two Random Variables is Stochastically Larger than the Other. Ann. Math. Stat. 18 (1), 50–60.
Mascia, M.M., Dagostino, S., Defazio, G., 2020. Does the network model fits neurophysiological abnormalities in blepharospasm? Neurol. Sci. 41 (8), 2067–2079.
Murai, H., Suzuki, Y., Kiyosawa, M., Wakakura, M., Mochizuki, M., Ishiwata, K., Ishii, K., 2011. Positive correlation between severity of blepharospasm and thalamic glucose metabolism. Case Rep. Ophthalmol. 2, 50–54.
Nair, A., Treiber, J.M., Shukla, D.K., Shih, P., Muller, R.A., 2013. Impaired thalamocortical connectivity in autism spectrum disorder: a study of functional and anatomical connectivity. Brain 136, 1942–1955.
Neychev, V.K., Gross, R.E., Lehéricy, S., Hess, E.J., Jinnah, H.A., 2011. The functional neuroanatomy of dystonia. Neurobiol. Dis. 42 (2), 185–201.
Nguyen, P., Kelly, D., Glickman, A., Argaw, S., Shelton, E., Peterson, D.A., Berman, B.D., 2020. Abnormal Neural Responses During Reflexive Blinking in Blepharospasm: An Event-Related Functional MRI Study. Mov. Disord. 35, 1173–1180.
Ni, M.F., Huang, X.F., Miao, Y.W., Liang, Z.H., 2017. Resting state fMRI observations of baseline brain functional activities and connectivities in primary blepharospasm. Neurosci. Lett. 660, 22–28.
Obermann, M., Yaldizli, O., de Greiff, A., Konczak, J., Lachenmayer, M.L., Tumczak, F., Buhl, A.R., Putzki, N., Vollmer-Haase, J., Gizewski, E.R., Diener, H.C., Maschke, M., 2008. Increased basal-ganglia activation performing a non-dystonia-related task in focal dystonia. Eur. J. Neurol. 15, 831–838.
Oldfield, R.C., 1971. The assessment and analysis of handedness: the Edinburgh inventory. Neuropsychologia 9 (1), 97–113.
Pandey, S., Sharma, S., 2017. Meige's syndrome: History, epidemiology, clinical features, pathogenesis and treatment. J. Neurol. Sci. 372, 162–170.
Quartarone, A., Hallett, M., 2013. Emerging concepts in the physiological basis of dystonia. Mov. Disord. 28 (7), 958–967.
Salimi-Khorshidi, G., Smith, S.M., Nichols, T.E., 2011. Adjusting the effect of nonstationarity in cluster-based and TFCE inference. Neuroimage 54 (3), 2006–2019.
Silkis, I., 2001. The cortico-basal ganglia-thalamocortical circuit with synaptic plasticity. II. Mechanism of synergistic modulation of thalamic activity via the direct and indirect pathways through the basal ganglia. Biosystems 59 (1), 7–14.
Smith, S., Nichols, T., 2009. Threshold-free cluster enhancement: addressing problems of smoothing, threshold dependence and localisation in cluster inference. Neuroimage 44 (1), 83–98.
Spearman, C., 1904. The proof and measurement of association between two things. Am. J. Psychol. 15, 72–101.
Suzuki, Y., Kiyosawa, M., Wakakura, M., Ishii, K., 2019. Glucose hypometabolism in the visual cortex proportional to disease severity in patients with essential blepharospasm. Neuroimage Clin 24, 101995.
Suzuki, Y., Mizoguchi, S., Kiyosawa, M., Mochizuki, M., Ishiwata, K., Wakakura, M., Ishii, K., 2007. Glucose hypermetabolism in the thalamus of patients with essential blepharospasm. J. Neurol. 254, 890–896.
Valls-Sole, J., Defazio, G., 2016. Blepharospasm: Update on Epidemiology, Clinical Aspects, and Pathophysiology. Front. Neurol. 7, 45.
van Eimeren, T., Boecker, H., Konkiewitz, E.C., Schwaiger, M., Conrad, B., Ceballos-Baumann, A.O., 2001. Right lateralized motor cortex activation during volitional blinking. Ann. Neurol. 49, 813–816.
Vo, A., Sako, W., Niethammer, M., Carbon, M., Bressman, S.B., Ulug, A.M., Eidelberg, D., 2015. Thalamocortical Connectivity Correlates with Phenotypic Variability in Dystonia. Cereb. Cortex 25, 3086–3094.
Winkler, A.M., Ridgway, G.R., Douaud, G., Nichols, T.E., Smith, S.M., 2016. Faster permutation inference in brain imaging. Neuroimage 141, 502–516.
Winkler, A.M., Ridgway, G.R., Webster, M.A., Smith, S.M., Nichols, T.E., 2014. Permutation inference for the general linear model. Neuroimage 92, 381–397.
Yang, J., Luo, C., Song, W., Guo, X., Zhao, B., Chen, X., Huang, X., Gong, Q., Shang, H.F., 2014. Diffusion tensor imaging in blepharospasm and blepharospasm-oromandibular dystonia. J. Neurol. 261, 1413–1424.
Yoon, H.W., Chung, J.Y., Song, M.S., Park, H., 2005. Neural correlates of eye blinking; improved by simultaneous fMRI and EOG measurement. Neurosci. Lett. 381, 26–30.
Zhang, D., Snyder, A.Z., Shimony, J.S., Fox, M.D., Raichle, M.E., 2010. Noninvasive functional and structural connectivity mapping of the human thalamocortical system. Cereb. Cortex 20, 1187–1194.